

# Pseudoscalar Higgs boson production associated with a single bottom quark at hadron colliders

---

Hou Hong-Sheng<sup>b</sup>, Ma Wen-Gan<sup>a,b</sup>, Zhang Ren-You<sup>b</sup>, Sun Yan-Bin<sup>b</sup> and Wu Peng<sup>b</sup>

<sup>a</sup>*CCAST (World Laboratory), P.O.Box 8730, Beijing, 100080, People's Republic of China*

<sup>b</sup>*Department of Modern Physics, University of Science and Technology of China (USTC), Hefei, Anhui 230027, People's Republic of China*

*Email: hhsheng@mail.ustc.edu.cn, mawg@ustc.edu.cn, zhangry@mail.ustc.edu.cn, sunyb@mail.ustc.edu.cn, and lily@mail.ustc.edu.cn*

**ABSTRACT:** We compute the complete next-to-leading order (NLO) SUSY-QCD corrections for the associated production of a pseudoscalar Higgs boson with a bottom quark via bottom-gluon fusion at the CERN Large Hadron Collider (LHC) and the Fermilab Tevatron. We find that the NLO QCD correction in the MSSM reaches 40%  $\sim$  50% at the LHC and 45%  $\sim$  80% at the Tevatron in our chosen parameter space.

**KEYWORDS:** Supersymmetry Phenomenology, Higgs Physics, NLO Computations, Hadronic Colliders.

---

## Contents

<b>1. Introduction</b>	<b>1</b>
<b>2. The leading order cross section</b>	<b>2</b>
<b>3. NLO QCD corrections</b>	<b>3</b>
3.1 Virtual Corrections	4
3.2 Real gluon emission corrections	6
<b>4. Numeric results and discussion</b>	<b>9</b>

---

## 1. Introduction

The standard model (SM) [1], with the Higgs mechanism manifested by a single complex scalar weak isospin doublet that spontaneously break the electrowak gauge symmetry, is believed to be an incomplete description of nature. There exists the problem of the quadratically divergent contributions to the corrections to the Higgs boson mass. This is the so-called naturalness problem of the SM. One of the good methods to solve this problem is to make supersymmetric (SUSY) extensions to the SM. The quadratic divergences of the Higgs mass can be cancelled by loop diagrams involving the supersymmetric partners of the SM particles exactly. The most attractive supersymmetric extension of the SM is the minimal supersymmetric standard model (MSSM) [2, 3]. Any enlargement of the sector beyond the single  $SU(2)_L$  Higgs doublet of SM, with two or more doublets as required in supersymmetric theory, necessarily involves new physical particles. In the MSSM, there are two Higgs doublets  $H_1^0$  and  $H_2^0$  to give masses to down- and up-type fermions. The Higgs sector consists of three neutral Higgs bosons, one  $CP$ -odd particle ( $A^0$ ), two  $CP$ -even particles ( $h^0$  and  $H^0$ ), and a pair of charged Higgs bosons ( $H^\pm$ ).

The discovery of the additional heavy Higgs bosons will help us to probe the contents of the supersymmetric Higgs sector. Until now all supersymmetric Higgs bosons haven't been directly explored yet, only LEP2 group presents the strongest lower mass limits of 91.0  $GeV$  and 91.9  $GeV$  for the light  $CP$ -even and the  $CP$ -odd neutral Higgs bosons  $h^0$  and  $A^0$ [4], respectively. The CERN Large Hadron Collider (LHC), which is a proton-proton collider with  $\sqrt{S} = 14 TeV$  and a luminosity of 100  $fb^{-1}$  per year, has been designed specifically to continue finding Higgs bosons. In the MSSM theory with a large value of  $\tan\beta$  ( $\tan\beta = v_2/v_1$ ,  $v_1$  and  $v_2$  are the vacuum expectation values of the two Higgs boson fields  $H_1^0$  and  $H_2^0$ , respectively), the strength of the  $A^0 b\bar{b}$  coupling increases greatly. The pseudoscalar Higgs boson  $A^0$  could be produced with a substantial rate at the LHC either in association with bottom quarks [ $q\bar{q}, gg \rightarrow b\bar{b}A^0$  or  $gb(\bar{b}) \rightarrow b(\bar{b})A^0$ ] or through  $gg \rightarrow A^0$

when  $b$  or  $\tilde{b}$  loops dominate, provided that  $\tan\beta$  is large enough[5]. Ref.[6] presents the calculation of the total cross section of the  $A^0$  plus two jets at the lowest order. The total cross section for the inclusive production of  $A^0$  has been calculated at NLO in Ref.[7] and at NNLO in Refs.[8][9], where the authors use the effective lagrangian for the interaction of  $A^0$  Higgs boson with the gluons and neglect the contribution of bottom quark loop so that their result is only for small and moderate value of  $\tan\beta$ .

Because the high- $p_T$  bottom quark can be tagged with reasonably high efficiency, the observation of a bottom quark with high  $p_T$  can reduce the backgrounds of the  $A^0$  Higgs boson production. The  $A^0$  Higgs boson production associated with bottom quark can occur via tree-level subprocess  $g\bar{b} \rightarrow b\bar{b}A^0$ [13], where the initial bottom quark resides in the proton sea. The cross section for the production of Higgs boson  $h^0$  and a single high  $p_T$  bottom quark via subprocess  $g\bar{b} \rightarrow b\bar{b}h^0$  has been studied in both QCD and SUSY-QCD at NLO [14, 15, 16]. However, it is pointed out in Ref.[10] that the calculation of  $\bar{b}\bar{b} \rightarrow h^0$  may overestimate the inclusive cross section with the introduction of conventional  $b$  densities, due to crude approximations inherent in the kinematics, which give rise to large bottom quark mass and phase space effect. But in Ref.[11], it is shown that the bottom parton approach is valid by choosing the appropriate factorization scale for the process  $\bar{b}\bar{b} \rightarrow h^0$  with  $\mu_f = m_h/4$  rather than  $m_h$ . In Ref.[12], the author computed the NLO contributions to the inclusive cross section  $pp \rightarrow tH^-$  via the subprocess  $bg \rightarrow tH^-$  and shown the bottom parton approach is valid for this process by choosing the factorization scale with about  $\mu_f \sim m_{av}/3 = (m_t + m_{H^-})/6$ . In our calculation, we choose the factorization scale as  $\mu_f = m_A/4$  when we use the bottom parton approximation.

In this paper, we calculated the cross section for the associated production of the  $A^0$  Higgs boson and a single high- $p_T$  bottom quark via  $bg \rightarrow A^0b$  ( $\bar{b}g \rightarrow A^0\bar{b}$ ) in the MSSM at the Tevatron and LHC including the NLO QCD corrections. The structure of this paper is as follow: In Sec. 2, we discuss the LO results of the subprocess  $bg \rightarrow A^0b$ . In Sec. 3, we present the calculations of the NLO QCD corrections. In Sec. 4, the numerical results and conclusions are presented.

## 2. The leading order cross section

Since the cross sections for the subprocess  $bg \rightarrow A^0b$  and its charge-conjugate subprocess  $\bar{b}g \rightarrow A^0\bar{b}$  in the CP-conserved MSSM are same, we present only the calculation of the subprocess  $b(p_1)g(p_2) \rightarrow A^0(k_3)b(k_4)$  here (where  $p_{1,2}$  and  $k_{3,4}$  represent the four-momentum of the incoming partons and the outgoing particles, respectively.). The subprocess  $bg \rightarrow A^0b$  can occur through both s-channel and t-channel as shown in Fig.1(A-B). So we divide the tree-level amplitude into two parts and denote it as

$$M^0 = M_0^{(s)} + M_0^{(t)}, \quad (2.1)$$

where  $M_0^{(s)}$  and  $M_0^{(t)}$  represent the amplitudes arising from the s-channel diagram shown in Fig.1(A) and the t-channel diagram shown in Fig.1(B) at the tree-level, respectively.

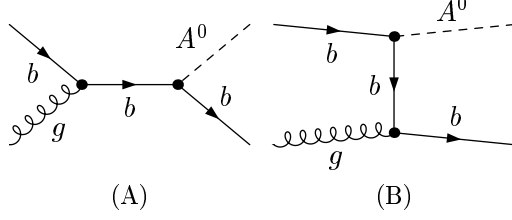


**Figure 1:** Leading order Feynman diagrams for the subprocess of  $bg \rightarrow A^0 b$

The explicit expressions for the amplitudes  $M_0^{(s)}$  and  $M_0^{(t)}$  can be written as

$$\begin{aligned}
 M_0^{(s)} &= \frac{g_s(\mu_r)V_{Abb}(\mu_r)}{\hat{s}} \bar{u}_i(k_4)\gamma_5(\not{p}_1 + \not{p}_2)\gamma_\nu u_j(p_1)\epsilon_\nu^a(p_2)T_{ij}^a, \\
 M_0^{(t)} &= \frac{g_s(\mu_r)V_{Abb}(\mu_r)}{\hat{t}} \bar{u}_i(k_4)\gamma_\nu(\not{p}_1 - \not{k}_3)\gamma_5 u_j(p_1)\epsilon_\nu^a(p_2)T_{ij}^a,
 \end{aligned}
 \tag{2.2}$$

where  $\hat{s} = (p_1 + p_2)^2$ ,  $\hat{t} = (p_1 - k_3)^2$  and  $\hat{u} = (p_1 - k_4)^2$  are the usual Mandelstam variables.  $\mu_r$  is the renormalization scale,  $g_s(\mu_r)$  is the running strong coupling strength and  $T^a$  is the  $SU(3)$  color matrix.  $V_{Abb}(\mu_r)\gamma_5$  is the Yukawa coupling between  $A^0$  Higgs boson and bottom quarks. In MSSM,  $V_{Abb}(\mu_r)$  is given as

$$V_{Abb}(\mu_r) = -\frac{g_w \overline{m}_b(\mu_r) \tan \beta}{2m_W}
 \tag{2.3}$$

$\overline{m}_b(\mu_r)$  is the  $\overline{\text{MS}}$  running mass of the bottom quark. It is well known that we should use the running mass rather than the pole mass when evaluation of the Yukawa coupling, because the pole mass Yukawa coupling will yield a huge overestimate of the cross section. Throughout our evaluation we neglect the bottom quark mass except in the Yukawa couplings. This corresponds to the simplified Aivazis-Collins-Olness-Tung(ACOT) scheme[19]. In any diagram in which the bottom quark is an initial-state parton, the bottom quark mass may be neglected without any loss of accuracy.

Then the lowest order cross section for the subprocess  $bg \rightarrow A^0 b$  in the MSSM is obtained by using the following formula:

$$\hat{\sigma}^0(\hat{s}, bg \rightarrow A^0 b) = \frac{1}{16\pi\hat{s}^2} \int_{\hat{t}_{min}}^{\hat{t}_{max}} d\hat{t} \overline{\sum} |M^0|^2,
 \tag{2.4}$$

where  $\hat{t}_{max} = 0$  and  $\hat{t}_{min} = m_A^2 - \hat{s}$ . The summation is taken over the spins and colors of initial and final states, and the bar over the summation recalls averaging over the spins and colors of initial partons.

### 3. NLO QCD corrections

The NLO QCD contributions to the subprocess  $bg \rightarrow A^0 b$  can be separated into two parts: the virtual corrections arising from loop diagrams and the real gluon emission corrections.

### 3.1 Virtual Corrections

The virtual corrections in the MSSM to  $bg \rightarrow A^0 b$  consist of self-energy, vertex and box diagrams which are shown in Figs.2-3. Fig.2 shows the one-loop diagrams of the SM-like QCD corrections from quarks and gluons, and Fig.3 presents the one-loop diagrams of the SUSY QCD corrections from squarks and gluinos. There exist both ultraviolet(UV) and soft/collinear infrared(IR) singularities in the amplitude from the SM-like diagrams in Fig.2, and the amplitude part from SUSY QCD diagrams(Fig.3) only contains UV singularities. In our calculation, we adopt the 't Hooft-Feynman gauge and all the divergences are regularized by using dimensional regularization method in  $d = 4 - 2\epsilon$  dimensions.

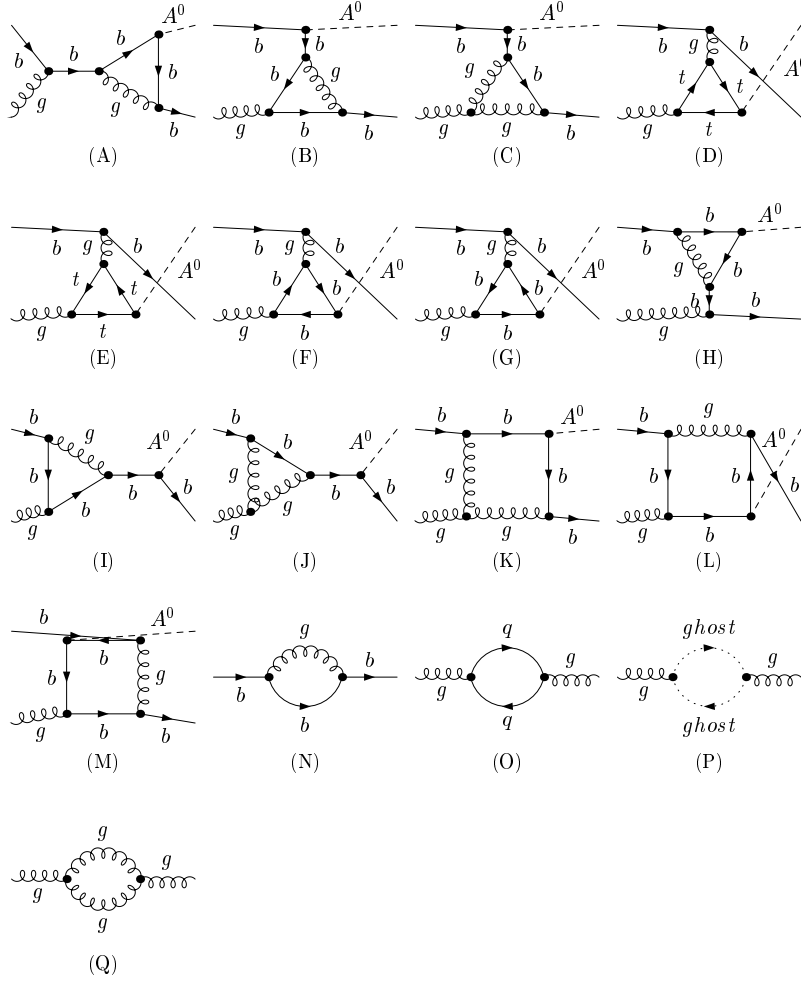


**Figure 2:** Virtual one-loop Feynman diagrams for the subprocess of  $bg \rightarrow A^0 b$  of the SM-like QCD corrections.

In order to remove the UV divergences, we need to renormalize the wave functions of the external fields, the strong coupling and the  $A^0 - b - \bar{b}$  Yukawa coupling. For the renormalization of the strong and Yukawa couplings, we employ the modified Minimal

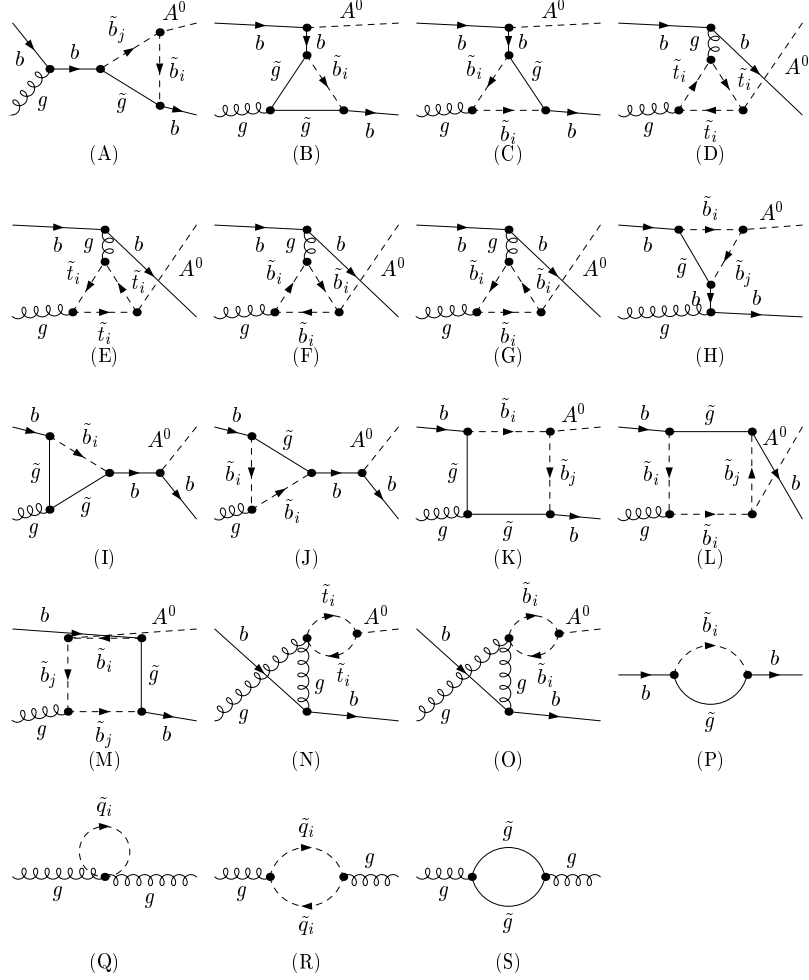


**Figure 3:** Virtual one-loop Feynman diagrams for the subprocess of  $bg \rightarrow A^0 b$  of the SUSY QCD corrections.

Subtraction ( $\overline{\text{MS}}$ ) scheme. The relevant renormalization constants in this work are defined same as those in Ref.[15].

The virtual corrections to the cross section can be written as

$$\hat{\sigma}^V(\hat{s}, bg \rightarrow A^0 b) = \frac{1}{16\pi\hat{s}^2} \int_{\hat{t}_{min}}^{\hat{t}_{max}} d\hat{t} \, 2\text{Re} \overline{\sum} [(M^V)^\dagger M^0], \quad (3.1)$$

with  $\hat{t}_{max} = 0$  and  $\hat{t}_{min} = m_A^2 - \hat{s}$  and again the summation<sup>1</sup>with bar means the same operations as appeared in Eq.(2.4).  $M^V$  is the renormalized amplitude for virtual corrections.

After the renormalization procedure,  $\hat{\sigma}^V$  is UV-finite. Nevertheless, it still contains the soft/collinear IR singularities

$$d\hat{\sigma}^V|_{IR} = \left[ \frac{\alpha_s}{2\pi} \frac{\Gamma(1-\epsilon)}{\Gamma(1-2\epsilon)} \left( \frac{4\pi\mu_r^2}{\hat{s}} \right)^\epsilon \right] d\hat{\sigma}^0 \left( \frac{A_2^V}{\epsilon^2} + \frac{A_1^V}{\epsilon} \right), \quad (3.2)$$

where

$$\begin{aligned}
A_2^V &= -\frac{17}{3}, \\
A_1^V &= -\frac{47}{6} + 3 \ln \frac{-\hat{t}}{\hat{s} - m_A^2} - \frac{1}{3} \ln \frac{-\hat{u}}{\hat{s} - m_A^2}.
\end{aligned}
\tag{3.3}$$

The soft divergences can be cancelled by adding with the soft real gluon emission corrections, and the remaining collinear divergences are absorbed into the parton distribution functions, which will be discussed in the next subsection.

### 3.2 Real gluon emission corrections

The  $O(\alpha_s)$  corrections to  $bg \rightarrow A^0 b$  due to real gluon emission (shown in Fig.4) give the origin of IR singularities which cancel exactly the analogous singularities present in the  $O(\alpha_s)$  virtual corrections mentioned in above subsection. These singularities can be either of soft or collinear nature and can be conveniently isolated by slicing the  $bg \rightarrow A^0 b + g$  phase space into different regions defined by suitable cutoffs, a method which goes under the general name of Phase Space Slicing(PPS).

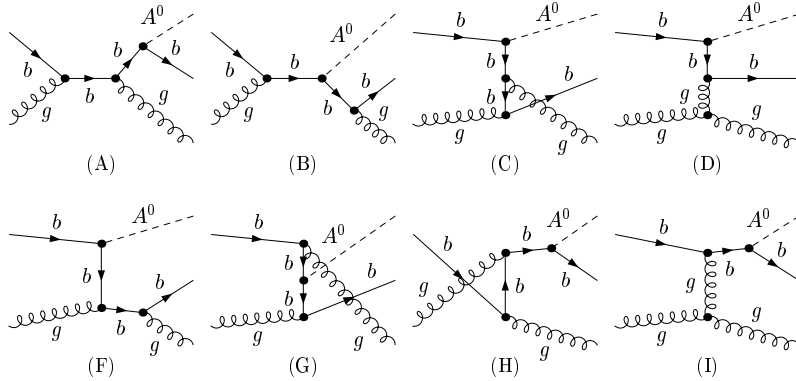


**Figure 4:** Feynman diagrams for the subprocess of  $bg \rightarrow A^0 bg$  with a real gluon emission.

In this paper, we calculate the cross section for the  $2 \rightarrow 3$  process

$$b(p_1) + g(p_2) \rightarrow A^0(k_3) + b(k_4) + g(k_5),
\tag{3.4}$$

adopting the method named two cutoff phase space slicing method[20]. We define the invariants

$$\begin{aligned}
\hat{s} &= (p_1 + p_2)^2, \quad \hat{t} = (p_1 - k_3)^2, \quad \hat{u} = (p_1 - k_4)^2, \\
\hat{s}_{45} &= (k_4 + k_5)^2, \quad \hat{t}_{15} = (p_1 - k_5)^2, \quad \hat{t}_{25} = (p_2 - k_5)^2, \quad \hat{t}_{45} = (k_4 - k_5)^2,
\end{aligned}
\tag{3.5}$$

and describe this method briefly as follows. Firstly, by introducing an arbitrary small soft cutoff  $\delta_s$  we separate the  $2 \rightarrow 3$  phase space into two regions, according to whether the

energy of the emitted gluon is soft, i.e.  $E_5 \leq \delta_s \sqrt{\hat{s}}/2$ , or hard, i.e.  $E_5 > \delta_s \sqrt{\hat{s}}/2$ . The partonic real cross section can be written as

$$\hat{\sigma}^R(bg \rightarrow A^0bg) = \hat{\sigma}^S(bg \rightarrow A^0bg) + \hat{\sigma}^H(bg \rightarrow A^0bg), \quad (3.6)$$

where  $\hat{\sigma}^S$  is obtained by integrating over the soft region of the emitted gluon phase space.  $\hat{\sigma}^S$  contains all the soft IR singularities. Secondly, to isolate the remaining collinear singularities from  $\hat{\sigma}^H$ , we further decompose  $\hat{\sigma}^H$  into a sum of hard-collinear (HC) and hard-non-collinear ( $\overline{\text{HC}}$ ) terms by introducing another cutoff  $\delta_c$  named collinear cutoff

$$\hat{\sigma}^H(bg \rightarrow A^0bg) = \hat{\sigma}^{\text{HC}}(bg \rightarrow A^0bg) + \hat{\sigma}^{\overline{\text{HC}}}(bg \rightarrow A^0bg). \quad (3.7)$$

The HC regions of the phase space are those where any invariant  $t_{15}, t_{25}, t_{45}$  becomes smaller in magnitude than  $\delta_c \hat{s}$ , in collinear condition, while at the same time the emitted gluon remains hard.  $\hat{\sigma}^{\text{HC}}$  contains the collinear divergences. In the soft and HC region,  $\hat{\sigma}^S$  and  $\hat{\sigma}^{\text{HC}}$  can be obtained by performing the phase space integration in  $d$ -dimension analytically. In the  $\overline{\text{HC}}$  region,  $\hat{\sigma}^{\overline{\text{HC}}}$  is finite and may be evaluated in four dimensions using standard Monte Carlo techniques[21]. The cross sections,  $\hat{\sigma}^S$ ,  $\hat{\sigma}^{\text{HC}}$  and  $\hat{\sigma}^{\overline{\text{HC}}}$ , depend on the two arbitrary parameters,  $\delta_s$  and  $\delta_c$ . However, in the total real gluon emission hadronic cross section  $\hat{\sigma}^R$ , after mass factorization, the dependence on these arbitrary cutoffs cancels, as will be explicitly shown in Sec. 4. This constitutes an important check of our calculation.

The soft region of the  $bg \rightarrow A^0b + g$  phase space is defined by

$$0 < E_5 \leq \delta_s \sqrt{\hat{s}}/2 \quad (3.8)$$

The differential cross section in the soft region is given as

$$d\hat{\sigma}^S = d\hat{\sigma}^0 \left[ \frac{\alpha_s}{2\pi} \frac{\Gamma(1-\epsilon)}{\Gamma(1-2\epsilon)} \left( \frac{4\pi\mu_r^2}{\hat{s}} \right)^\epsilon \right] \left( \frac{A_2^S}{\epsilon^2} + \frac{A_1^S}{\epsilon} + A_0^S \right), \quad (3.9)$$

with

$$\begin{aligned} A_2^S &= \frac{17}{3}, \\ A_1^S &= -\frac{34}{3} \ln \delta_s - 3 \ln \frac{-\hat{t}}{\hat{s} - m_A^2} + \frac{1}{3} \ln \frac{-\hat{u}}{\hat{s} - m_A^2}, \\ A_0^S &= \frac{34}{3} \ln^2 \delta_s + 6 \ln \delta_s \ln \frac{-\hat{t}}{\hat{s} - m_A^2} + \frac{3}{2} \ln^2 \frac{-\hat{t}}{\hat{s} - m_A^2} \\ &\quad - \frac{2}{3} \ln \delta_s \ln \frac{-\hat{u}}{\hat{s} - m_A^2} - \frac{1}{6} \ln^2 \frac{-\hat{u}}{\hat{s} - m_A^2} - \frac{1}{3} Li_2 \left[ \frac{-\hat{t}}{\hat{s} - m_A^2} \right] + 3 Li_2 \left[ \frac{-\hat{u}}{\hat{s} - m_A^2} \right]. \end{aligned} \quad (3.10)$$

In the limit where two of the partons are collinear, the three body phase space is greatly simplified. And in the same limit, the leading pole approximation of the matrix element is valid. According to whether the collinear singularities are initial or final state in origin, we separate  $\hat{\sigma}^{\text{HC}}$  into two pieces

$$\hat{\sigma}^{\text{HC}} = \hat{\sigma}_i^{\text{HC}} + \hat{\sigma}_f^{\text{HC}}. \quad (3.11)$$



$\hat{\sigma}_i^{\text{HC}}$  is the cross section arising from the case that the emitted gluon is collinear to the initial partons,  $0 \leq t_{15}, t_{25} \leq \delta_c \hat{s}$ . And  $\hat{\sigma}_f^{\text{HC}}$  arises from the case that the emitted gluon is collinear to the final parton,  $0 \leq t_{45} \leq \delta_c \hat{s}$ .

The cross section  $\hat{\sigma}_f^{\text{HC}}$  can be written as

$$d\hat{\sigma}_f^{\text{HC}} = d\hat{\sigma}^0 \left[ \frac{\alpha_s}{2\pi} \frac{\Gamma(1-\epsilon)}{\Gamma(1-2\epsilon)} \left( \frac{4\pi\mu_r^2}{\hat{s}} \right)^\epsilon \right] \left( \frac{A_1^{b \rightarrow bg}}{\epsilon} + A_0^{b \rightarrow bg} \right), \quad (3.12)$$

where

$$\begin{aligned} A_1^{b \rightarrow bg} &= C_F(3/2 + 2 \ln \delta_s), \\ A_0^{b \rightarrow bg} &= C_F[7/2 - \pi^2/3 - \ln^2 \delta_s - \ln \delta_c(3/2 + 2 \ln \delta_s)]. \end{aligned} \quad (3.13)$$

The cross section  $\sigma_i^{\text{HC}}$  can be written as

$$\begin{aligned} d\sigma_i^{\text{HC}} &= d\hat{\sigma}^0 \left[ \frac{\alpha_s}{2\pi} \frac{\Gamma(1-\epsilon)}{\Gamma(1-2\epsilon)} \left( \frac{4\pi\mu_r^2}{\hat{s}} \right)^\epsilon \right] \left( -\frac{1}{\epsilon} \right) \delta_c^{-\epsilon} [P_{bb}(z, \epsilon) G_{b/A}(x_1/z) G_{g/B}(x_2) \\ &+ P_{gg}(z, \epsilon) G_{g/A}(x_1/z) G_{b/B}(x_2) + (x_1 \leftrightarrow x_2)] \frac{dz}{z} \left( \frac{1-z}{z} \right)^{-\epsilon} dx_1 dx_2. \end{aligned} \quad (3.14)$$

where  $G_{b,g/A,B}(x)$  is the bare parton distribution function,  $P_{bb}(z, \epsilon)$  and  $P_{gg}(z, \epsilon)$  are the  $d$ -dimensional unregulated ( $z < 1$ ) splitting function related to the usual Altarelli-Parisi splitting kernels[22].  $P_{ii}(z, \epsilon)$  ( $i = b, g$ ) can be written explicitly as

$$\begin{aligned} P_{ii}(z, \epsilon) &= P_{ii}(z) + \epsilon P'_{ii}(z) \quad (i = b, g), \\ P_{bb}(z) &= C_F \frac{1+z^2}{1-z}, \quad P'_{bb}(z) = -C_F(1-z) \\ P_{gg}(z) &= 2N \left[ \frac{z}{1-z} + \frac{1-z}{z} + z(1-z) \right], \quad P'_{gg}(z) = 0. \end{aligned} \quad (3.15)$$

with  $N = 3$  and  $C_F = 4/3$ .

In order to factorize the collinear singularity of  $\sigma_i^{\text{HC}}$  into the parton distribution function, we introduce a scale dependent parton distribution function using the  $\overline{\text{MS}}$  convention:

$$G_{i/A}(x, \mu_f) = G_{i/A}(x) + \left( -\frac{1}{\epsilon} \right) \left[ \frac{\alpha_s}{2\pi} \frac{\Gamma(1-\epsilon)}{\Gamma(1-2\epsilon)} \left( \frac{4\pi\mu_r^2}{\mu_f^2} \right)^\epsilon \right] \int_z^1 \frac{dz}{z} P_{ii}(z) G_{i/A}(x/z), \quad (i = b, g). \quad (3.16)$$

By using above definition, we replace  $G_{g,b/A,B}$  in Eq.(3.14) and the expression for the initial state collinear contribution at  $O(\alpha_s)$  order is

$$\begin{aligned} d\sigma_i^{\text{HC}} &= d\hat{\sigma}^0 \left[ \frac{\alpha_s}{2\pi} \frac{\Gamma(1-\epsilon)}{\Gamma(1-2\epsilon)} \left( \frac{4\pi\mu_r^2}{\hat{s}} \right)^\epsilon \right] \{ \tilde{G}_{g/A}(x_1, \mu_f) G_{b/B}(x_2, \mu_f) + G_{g/A}(x_1, \mu_f) \tilde{G}_{b/B}(x_2, \mu_f) \\ &+ \sum_{\alpha=g,b} \left[ \frac{A_1^{\text{sc}}(\alpha \rightarrow \alpha g)}{\epsilon} + A_0^{\text{sc}}(\alpha \rightarrow \alpha g) \right] G_{g/A}(x_1, \mu_f) G_{b/B}(x_2, \mu_f) \\ &+ (x_1 \leftrightarrow x_2) \} dx_1 dx_2, \end{aligned} \quad (3.17)$$

where

$$\begin{aligned}
A_1^{sc}(b \rightarrow bg) &= C_F(2 \ln \delta_s + 3/2), \\
A_1^{sc}(g \rightarrow gg) &= 2N \ln \delta_s + (11N - 2n_f)/6, \\
A_0^{sc} &= A_1^{sc} \ln\left(\frac{\hat{s}}{\mu_f^2}\right).
\end{aligned} \tag{3.18}$$

And

$$\tilde{G}_{\alpha/A,B}(x, \mu_f) = \int_x^{1-\delta_s} \frac{dy}{y} G_{\alpha/A,B}(x/y, \mu_f) \tilde{P}_{\alpha\alpha}(y), \quad (\alpha = g, b), \tag{3.19}$$

with

$$\tilde{P}_{\alpha\alpha}(y) = P_{\alpha\alpha} \ln\left(\delta_c \frac{1-y}{y} \frac{\hat{s}}{\mu_f^2}\right) - P'_{\alpha\alpha}(y), \quad (\alpha = g, b). \tag{3.20}$$

We can observe that the sum of the soft (Eq.(3.9)), collinear(Eq.(3.12),(3.17)), and ultra-violet renormalized virtual correction (Eq.(3.2)) terms is finite, i.e.,

$$\begin{aligned}
A_2^S + A_2^V &= 0, \\
A_1^S + A_1^V + A_1^{b \rightarrow bg} + A_1^{sc}(b \rightarrow bg) + A_1^{sc}(g \rightarrow gg) &= 0.
\end{aligned} \tag{3.21}$$

The final result for the  $O(\alpha_s)$  correction consists of two contributions to the cross section: a two-body term  $\sigma^{(2)}$  and a three-body term  $\sigma^{(3)}$ .

$$\begin{aligned}
\sigma^{(2)} &= \frac{\alpha_s}{2\pi} \int dx_1 dx_2 d\hat{\sigma}^0 \{G_{g/A}(x_1, \mu_f) G_{b/B}(x_2, \mu_f) [A_0^S + A_0^V + A_0^{b \rightarrow bg} + A_0^{sc}(b \rightarrow bg) + A_0^{sc}(g \rightarrow gg)] \\
&\quad + \tilde{G}_{g/A}(x_1, \mu_f) G_{b/B}(x_2, \mu_f) + G_{g/A}(x_1, \mu_f) \tilde{G}_{b/B}(x_2, \mu_f) + (x_1 \leftrightarrow x_2)\}.
\end{aligned} \tag{3.22}$$

And

$$\sigma^{(3)} = \int dx_1 dx_2 [G_{g/A}(x_1, \mu_f) G_{b/B}(x_2, \mu_f) + (x_1 \leftrightarrow x_2)] d\hat{\sigma}^{(3)}, \tag{3.23}$$

with the hard-non-collinear partonic cross section given by

$$d\hat{\sigma}^{(3)} = \frac{1}{2\hat{s}_{12}} \int_{\text{HC}} \sum |M_3(bg \rightarrow A^0 bg)|^2 d\Gamma_3. \tag{3.24}$$

Finally, the NLO total cross section for  $pp(\text{or } p\bar{p}) \rightarrow bA^0 + X$  is

$$\sigma^{NLO} = \sigma^0 + \sigma^{(2)} + \sigma^{(3)}. \tag{3.25}$$

#### 4. Numeric results and discussion

In the following numerical evaluation, we present the results of the cross section for the pseudoscalar Higgs boson production associated with a single high- $p_T$  bottom quark via subprocess  $bg(\bar{b}g) \rightarrow A^0 b(A^0 \bar{b})$  at the LHC and Tevatron. At the LHC, the  $b$ -jet is required to have a transverse momentum cut  $p_T(b) > 30 \text{ GeV}$  and a rapidity cut  $|\eta(b)| < 2.5$ . At

the Tevatron, the  $b$  tagging regions are taken to be  $|\eta(b)| < 2$  and  $p_T(b) > 15 \text{ GeV}$ . The SM parameters are taken as:  $m_t = 174.3 \text{ GeV}$ ,  $m_Z = 91.188 \text{ GeV}$ ,  $m_W = 80.419 \text{ GeV}$  and  $\alpha_{EW} = 1/128$  [23]. The factorization scale is taken as  $\mu_f = m_A/4$  and the renormalization scale is taken as  $\mu_r = m_A$ . We use the one-loop formula for the running strong coupling constant  $\alpha_s$  with  $\alpha_s(m_Z) = 0.117$ .

The relevant MSSM parameters in our calculation are: the parameters  $M_{\tilde{Q},\tilde{U},\tilde{D}}$  and  $A_{t,b}$  in squark mass matrices, the higgsino mass parameter  $\mu$ , the masses of the gluino  $m_{\tilde{g}}$  and the  $A^0$  Higgs boson  $m_A$ , the ratio of the vacuum expectation values of the two Higgs doublets  $\tan\beta$ . The squark mass matrix is defined as

$$\mathcal{M}_{\tilde{q}}^2 = \begin{pmatrix} m_{\tilde{q}L}^2 & a_q m_q \\ a_q m_q & m_{\tilde{q}R}^2 \end{pmatrix} \quad (4.1)$$

with

$$\begin{aligned} m_{\tilde{q}L}^2 &= M_{\tilde{Q}}^2 + m_q^2 + m_Z^2 \cos 2\beta (I_3^q - e_q \sin^2 \theta_W), \\ m_{\tilde{q}R}^2 &= M_{\{\tilde{U},\tilde{D}\}}^2 + m_q^2 + m_Z^2 \cos 2\beta e_q \sin^2 \theta_W \\ a_q &= A_q - \mu \{\cot \beta, \tan \beta\}, \end{aligned} \quad (4.2)$$

for {up, down} type squarks.  $I_3^q$  and  $e_q$  are the third component of the weak isospin and the electric charge of the quark  $q$ . The chiral states  $\tilde{q}_L$  and  $\tilde{q}_R$  are transformed into the mass eigenstates  $\tilde{q}_1$  and  $\tilde{q}_2$ :

$$\begin{pmatrix} \tilde{q}_1 \\ \tilde{q}_2 \end{pmatrix} = R^{\tilde{q}} \begin{pmatrix} \tilde{q}_L \\ \tilde{q}_R \end{pmatrix}, \quad R^{\tilde{q}} = \begin{pmatrix} \cos \theta_{\tilde{q}} & \sin \theta_{\tilde{q}} \\ -\sin \theta_{\tilde{q}} & \cos \theta_{\tilde{q}} \end{pmatrix}. \quad (4.3)$$

Then the mass eigenvalues  $m_{\tilde{q}_1}$  and  $m_{\tilde{q}_2}$  are given by

$$\begin{pmatrix} m_{\tilde{q}_1}^2 & 0 \\ 0 & m_{\tilde{q}_2}^2 \end{pmatrix} = R^{\tilde{q}} \mathcal{M}_{\tilde{q}}^2 (R^{\tilde{q}})^\dagger \quad (4.4)$$

For simplicity, we assume  $M_{\tilde{Q}} = M_{\tilde{U}} = M_{\tilde{D}} = A_t = A_b = m_{\tilde{g}}$  collectively denoted by  $M_{SUSY}$ .

In our calculation, we use the CTEQ5L parton distribution functions[25]. The  $\overline{\text{MS}}$  bottom quark mass  $\overline{m}_b$  can be evaluated by using the next-leading order formula [26]. In the following equations, we use  $\overline{m}_b(Q)$  to denote the  $\overline{\text{MS}}$  bottom quark mass.

$$\begin{aligned} \overline{m}_b(Q) &= U_5(Q, \overline{m}_b) \overline{m}_b(\overline{m}_b), \quad \text{for } Q < m_t, \\ \overline{m}_b(Q) &= U_6(Q, m_t) U_5(m_t, \overline{m}_b) \overline{m}_b(\overline{m}_b), \quad \text{for } Q > m_t, \end{aligned} \quad (4.5)$$

where  $\overline{m}_b = \overline{m}_b(\overline{m}_b) = 4.3 \text{ GeV}$ . The evolution factor  $U_f (f = 5, 6)$  is

$$\begin{aligned} U_f(Q_2, Q_1) &= \left( \frac{\alpha_s(Q_2)}{\alpha_s(Q_1)} \right)^{d^{(f)}} \left[ 1 + \frac{\alpha_s(Q_1) - \alpha_s(Q_2)}{4\pi} J^{(f)} \right], \\ d^{(f)} &= \frac{12}{33 - 2f}, \quad J^{(f)} = -\frac{8982 - 504f + 40f^2}{3(33 - 2f)^2} \end{aligned} \quad (4.6)$$

In the supersymmetry limit, bottom quarks only couple to the neutral Higgs doublet  $H_1^0$ . However, supersymmetry is broken and the bottom quark will receive a small coupling to the Higgs doublet  $H_2^0$  from radiative corrections. Considering these corrections,  $A^0$  Higgs boson coupling to the bottom quarks is given as [27]

$$-\overline{m}_b \frac{g_w \tan \beta}{2m_W} \gamma_5 \rightarrow -\frac{\overline{m}_b}{1 + \Delta_b} \frac{g_w \tan \beta}{2m_W} \gamma_5 \quad (4.7)$$

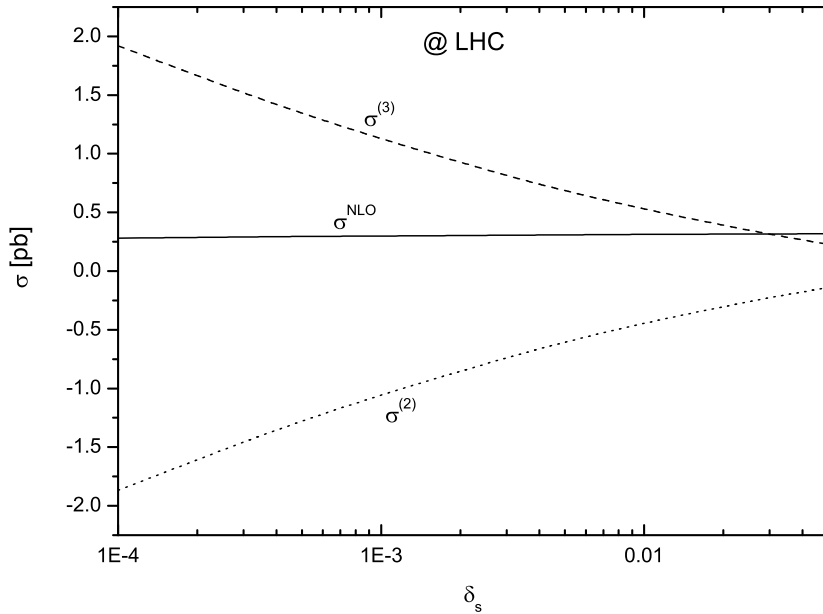
The explicit form of  $\Delta_b$  at one-loop is given by [28, 29, 30]

$$\Delta_b = \frac{2\alpha_s}{3\pi} m_{\tilde{g}} \tan \beta I(m_{\tilde{b}_1}, m_{\tilde{b}_2}, m_{\tilde{g}}) + \frac{h_t^2}{16\pi^2} A_t \mu \tan \beta I(m_{\tilde{t}_1}, m_{\tilde{t}_2}, \mu), \quad (4.8)$$

where  $h_t = \frac{\sqrt{2}m_t}{v \sin \beta}$ ,  $v = 246 \text{ GeV}$  and the function  $I$  is given by

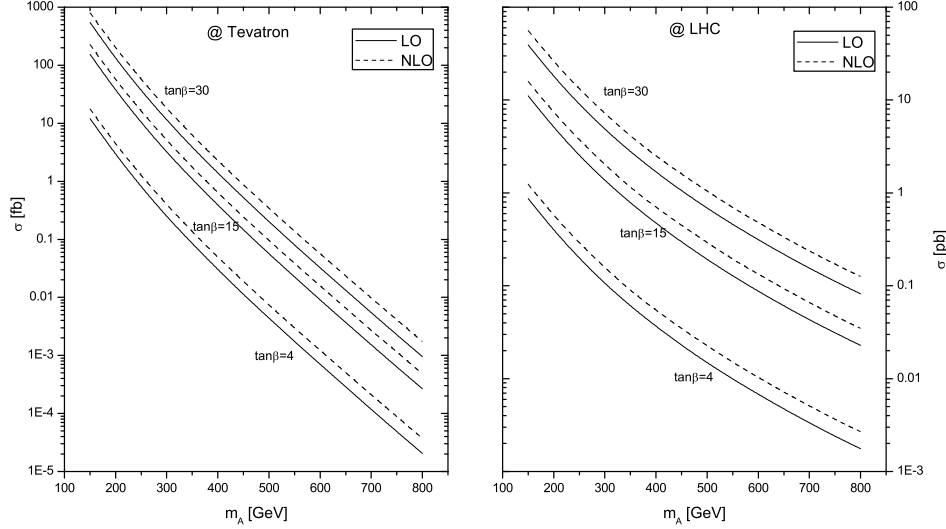
$$I(a, b, c) = \frac{1}{(a^2 - b^2)(b^2 - c^2)(a^2 - c^2)} (a^2 b^2 \log \frac{a^2}{b^2} + b^2 c^2 \log \frac{b^2}{c^2} + c^2 a^2 \log \frac{c^2}{a^2}). \quad (4.9)$$

Fig.5 shows that our NLO-QCD result does not depend on the arbitrary cutoffs  $\delta_s$  and  $\delta_c$  by using the two cutoff phase space slicing method. The two-body( $\sigma^{(2)}$ ) and three-body( $\sigma^{(3)}$ ) cross sections and the NLO cross section ( $\sigma^{NLO}$ ) at the LHC, are shown as the functions of the soft cutoff  $\delta_s$  with the collinear cutoff  $\delta_c = \delta_s/50$ . The supersymmetric parameters are taken as  $\mu = m_A = 200 \text{ GeV}$ ,  $M_{SUSY} = 500 \text{ GeV}$  and  $\tan \beta = 4$ . We can see the NLO cross section  $\sigma^{NLO}$  is independent of the cutoffs. In the following numerical calculations, we take  $\delta_s = 10^{-4}$  and  $\delta_c = \delta_s/50$ .



**Figure 5:** Dependence of the cross sections for the  $A^0 b$  production at the LHC on the cutoff  $\delta_s$  with  $\delta_c = \delta_s/50$ .

Fig.6 shows the dependence of the LO and NLO cross sections of the process  $pp$  (or  $p\bar{p}$ )  $\rightarrow bg(\bar{b}g) \rightarrow A^0b(A^0\bar{b}) + X$  at the LHC and Tevatron on the mass of  $A^0$  Higgs boson ( $m_A$ ). Here we take  $\mu = 200 \text{ GeV}$ ,  $M_{SUSY} = 500 \text{ GeV}$  and  $\tan\beta = 4, 15, 30$ . The relative NLO-QCD corrections are about 40%  $\sim$  50% at the LHC and about 45%  $\sim$  80% at the Tevatron when  $m_A$  varies from 200  $\text{GeV}$  to 800  $\text{GeV}$  for all the values of  $\tan\beta$  we have taken.



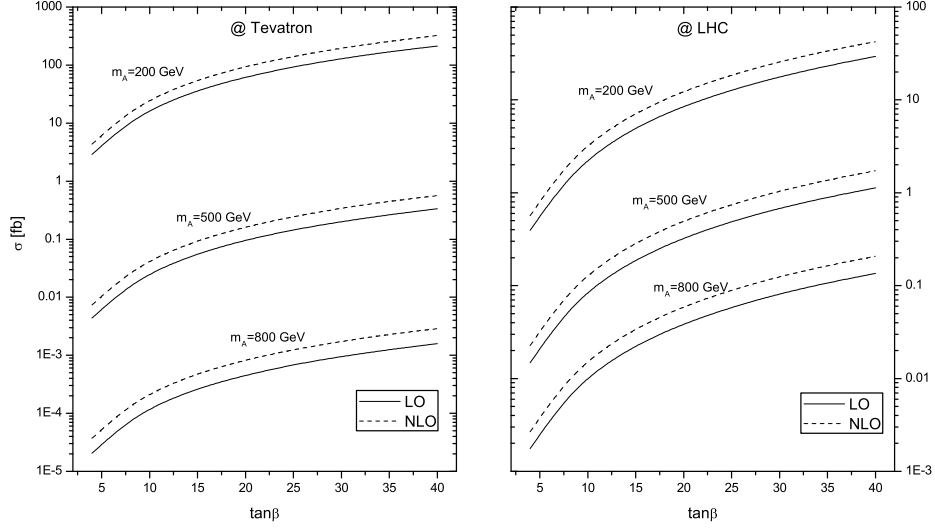
**Figure 6:** The dependence of the cross sections of process  $pp$  (or  $p\bar{p}$ )  $\rightarrow bg(\bar{b}g) \rightarrow A^0b(A^0\bar{b}) + X$  on the  $m_A$  with  $\tan\beta = 4, 15, 30$  at the LHC and Tevatron.

Fig.7 shows the cross sections of the process  $pp$  (or  $p\bar{p}$ )  $\rightarrow bg(\bar{b}g) \rightarrow A^0b(A^0\bar{b}) + X$  at the LHC and Tevatron as the functions of the ratio of the expectation vacuum values  $\tan\beta$ . We take  $\mu = 200 \text{ GeV}$ ,  $M_{SUSY} = 500 \text{ GeV}$  and  $m_A = 200, 500, 800 \text{ GeV}$ . Since the coupling between  $A^0$  Higgs boson and bottom quarks is greatly enhanced with large  $\tan\beta$  (see Eq.(2.3), Eq.(4.7)), the cross section of process  $pp$  (or  $p\bar{p}$ )  $\rightarrow bg(\bar{b}g) \rightarrow A^0b(A^0\bar{b}) + X$  at the LHC and Tevatron can be rather large. We can see that the cross section of the process  $pp$  (or  $p\bar{p}$ )  $\rightarrow bg(\bar{b}g) \rightarrow A^0b(A^0\bar{b}) + X$  can reach dozens of pico bar (or about 1  $pb$ ) when  $m_A = 200 \text{ GeV}$  and  $\tan\beta = 40$  (or when  $m_A = 500 \text{ GeV}$  and  $\tan\beta = 40$ ) at the LHC, while the cross section can be 200  $fb$  when  $m_A = 200 \text{ GeV}$  and  $\tan\beta = 40$  at the Tevatron.

In order to study the decoupling behavior of SUSY QCD correction, we push  $M_{SUSY}$  to a large value. The relative SUSY QCD correction is defined as

$$\Delta_{SQCD} = \frac{\delta\sigma^{SQCD}}{\sigma^0}, \quad (4.10)$$

where  $\delta\sigma^{SQCD}$  is the cross section correction contributed by the SUSY QCD diagrams shown in Fig.3. In Fig.8, we depict the relative SUSY QCD correction  $\Delta_{SQCD}$  as the functions of  $M_{SUSY}$  at the LHC. The relative SUSY QCD correction is small (about 2.2%  $\sim$  2.5%) but not vanishing with  $M_{SUSY}$  up to 2  $TeV$ .



**Figure 7:** The dependence of the cross sections of process  $pp$  (or  $p\bar{p}$ )  $\rightarrow bg(\bar{b}g) \rightarrow A^0 b(A^0 \bar{b}) + X$  on  $\tan\beta$  with  $m_A = 200, 500, 800\text{GeV}$  at the LHC and Tevatron.

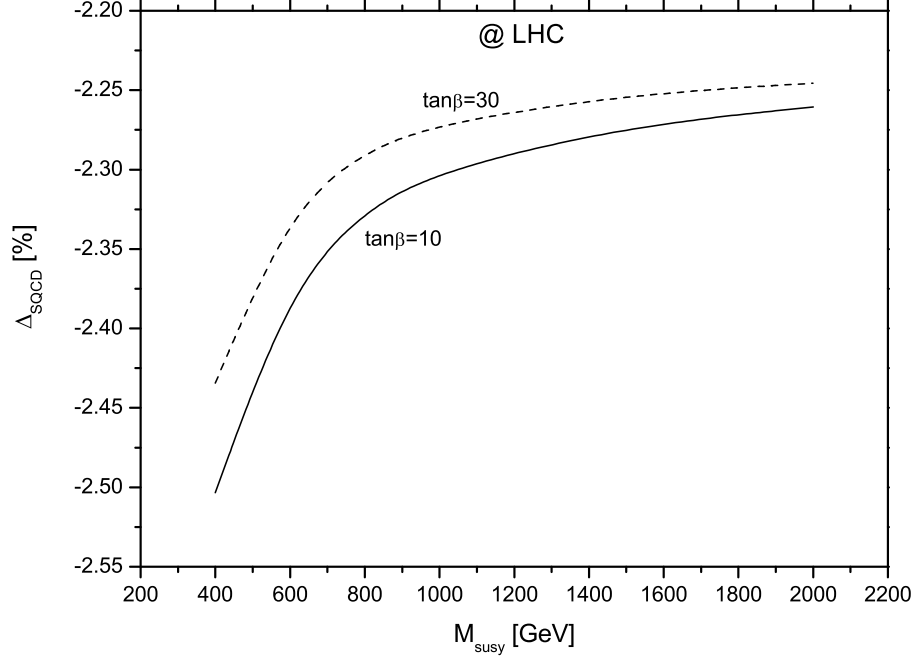


**Figure 8:** The dependence of  $\Delta_{SQCD}$  of process  $pp \rightarrow bg(\bar{b}g) \rightarrow A^0 b(A^0 \bar{b}) + X$  on  $M_{SUSY}$  at the LHC.

To analyze the scale dependence of the cross sections, We introduce the ratio of the cross section at scale  $\mu$  and the cross section at scale  $\mu = m_A$  and depict the  $\sigma(\mu)/\sigma(\mu = m_A)$  as a function of  $\mu/m_A$  at the LHC in Fig.9. For the solid lines, we fix the renormalization scale  $\mu_r = m_A$  and only show factorization scale  $\mu_f$  dependence of the cross sections.

For dashed lines,  $\mu_f$  and  $\mu_r$  are taken to be identical, vary from  $m_A/5$  to  $2m_A$ . The scale variation of the NLO-QCD cross section may be serves as an estimate of the remaining theoretical uncertainty of the high order corrections. Fig.9 shows that it is evident that the one-loop NLO-QCD corrections reduce the LO scale dependence for both the cases.

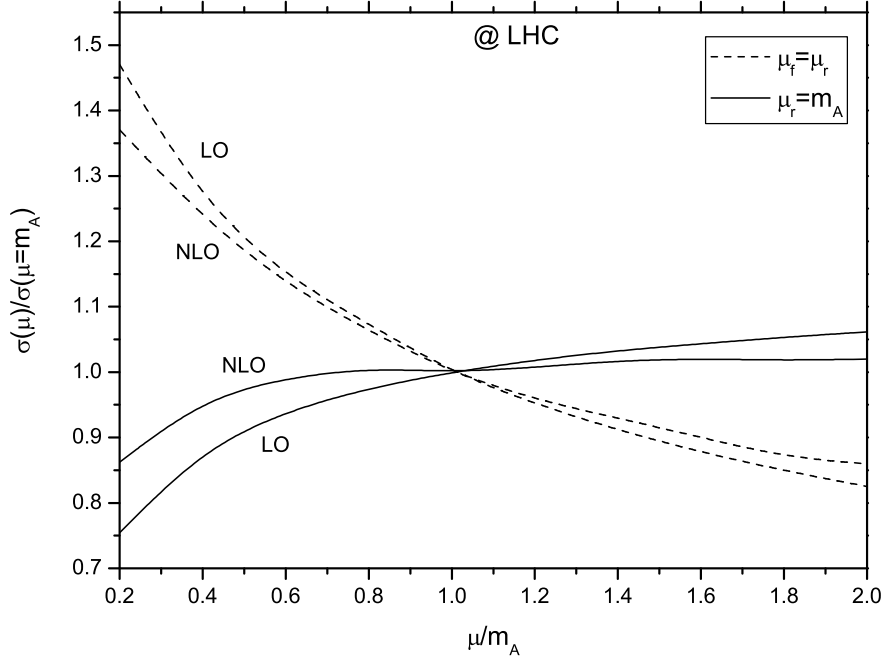


**Figure 9:** The variation of the  $\sigma(\mu)/\sigma(\mu = m_A)$  with the ratio  $\mu/m_A$  of process  $pp \rightarrow bg(\bar{b}g) \rightarrow A^0 b(A^0 \bar{b}) + X$  at the LHC.

In summary, we have computed the production of pseudoscalar Higgs boson  $A^0$  associated with a single high- $p_T$  bottom quark via subprocess  $bg(\bar{b}g) \rightarrow A^0 b(A^0 \bar{b})$  including the NLO-QCD corrections in the MSSM at the LHC and Tevatron. We find that due to the enhancement of the Yukawa coupling strength of the bottom quarks with  $A^0$  Higgs bosons at large  $\tan\beta$ , the cross section of the  $pp$  (or  $p\bar{p}$ )  $\rightarrow A^0 b(A^0 \bar{b})$  can reach dozens of pico bar at the LHC and hundreds of fermi bar at the Tevatron. The NLO-QCD corrections vary between 40%  $\sim$  50% at the LHC and 45%  $\sim$  80% at the Tevatron respectively, in the parameter space we have chosen.

**Acknowledgments.** This work was supported in part by the National Natural Science Foundation of China and a grant from the University of Science and Technology of China.

## References

- [1] S. Weinberg, Phys. Rev. Lett. **19**, 1264 (1967); S. Glashow, Nucl. Phys. **B22**, 579 (1961); A. Salam, in *Elementary Particle Theory*, edited by N. Svartholm (Almqvist and Wiksells, Stockholm, 1968), p.367.

- [2] H. P. Nilles Phys. Rep. **110**, 1 (1984); H. E. Haber and G. L. Kane, Phys. Rep. **117**, 75 (1985).
- [3] J. F. Gunion, H. E. Haber, Nucl. Phys. **B272**, 1 (1986).
- [4] ‘Searches for the Neutral Higgs Bosons of the MSSM: Preliminary Combined Results Using LEP Data Collected at Energies up to 209 GeV’, Aleph, Delphi, L3 and OPAL Collaborations, The LEP working group, LHWG Note 2002-04, Submitted to EPS’01 in Budapest and Lepton-Photon ’01 in Rome, hep-ex/0107030.
- [5] J. Conway, K. Desch, J.F. Gunion, S. Mrenna, and D. Zeppenfeld, eConf, C010630: P1WG2 (2001).
- [6] R. P. Kauffman and S. V. Desai, Phys. Rev. **D59** 057504(1999).
- [7] R. P. Kauffman and W. Schaffer, Phys. Rev. **D49**, 551(1994).
- [8] C. Anastasiou and K. Melnikov, Phys. Rev. **D67**, 037501(2003).
- [9] R. V. Harlander and W. B. Kilgore, JHEP10 (2002)017.
- [10] D. Rainwater, M. Spira and D. Zeppenfeld, arXiv:hep-ph/0203187; M. Spira, arXiv:hep-ph/0211145.
- [11] F. Maltoni, Z. Sullivan and S. Willenbrock, Phys. Rev. D **67**, 093005(2003).
- [12] T. Plehn, Phys. Rev. D **67**, 014018(2003).
- [13] C.S. Huang and S. H. Zhu, Phys. Rev. D **60**, 075012 (1999).
- [14] J. Campbell, R.K. Ellis, F. Maltoni and S. Willenbrock, Phys. Rev. **D67**, 095002 (2003).
- [15] H.S. Hou, W.G. Ma, P. Wu, L. Wang and R.Y. Zhang, Phys. Rev. D **68**,(2003)035016.
- [16] Junjie Cao, Guangping Gao, Robert J. Oakes, Jin Min Yang, arXiv:hep-ph/0210211.
- [17] A. Stange, W. Marciano and S. Willenbrock, Phys. Rev. **D49**, 1354 (1994).
- [18] D.A. Dicus and S. Willenbrock, Phys. Rev. **D39**, 751 (1989).
- [19] M.A.G. Aivazis, J.C. Collins, F.I. Olness, and W.K. Tung, Phys. Rev. **D50** 3102 (1994); J.C. Collins, Phys. Rev. **D58** 094002 (1998); M. Kramer, F.I. Olness, D.E. Soper, Phys. Rev. D **62** 096007 (2000).
- [20] B.W. Harris and J.F. Owens, Phys. Rev. D **65** 094032(2002).
- [21] G.P. Lepage, J. Comput. Phys. **27**,192(1978).
- [22] G. Altarelli and G. Parisi, Nucl. Phys. **B126** 298 (1977).
- [23] Particle Data Group, D.E. Groom *et al.*, Eur. Phys. J. **C15**, 1(2000).
- [24] S. Heinemeyer, W. Hollik and G. Weiglein, CERN-TH/2000-55, DESY 00-020, KA-TP-3-2000, arXiv:hep-ph/0002213.
- [25] H. L. Lai *et al.* [CTEQ Collaboration], Eur. Phys. J. **C12**, 375(2000).
- [26] M. Carena, D. Garcia, U. Nierste and C.E. Wagner, Nucl. Phys. **B577**, 88 (2000).
- [27] M. Carena, S. Mrenna, and C.E.M. Wagner, Phys. Rev. **D60** (1999) 075010.
- [28] L. Hall, R. Rattazzi and U. Sarid, Phys. Rev. **D50**(1994) 7048; R. Hempfling, Phys. Rev. **D49** (1994) 6168.
- [29] M. Carena, M. Olechowski, S. Pokorski and C.E.M. Wagner, Nucl. Phys. **B426** (1994)269.
- [30] D. Pierce, J. Bagger, K. Matchev, and R. Zhang, Nucl. Phys. **B491** (1997)3.